AFRL-ML-WP-TP-2006-454

SILVER DIFFUSION AND HIGH-TEMPERATURE LUBRICATION MECHANISMS OF YSZ-Ag-Mo BASED NANOCOMPOSITE COATINGS (Preprint)

J.J. Hu, C. Muratore, and A.A. Voevodin

MAY 2006

STINFO COPY

**MATERIALS AND MANUFACTURING DIRECTORATE
AIR FORCE RESEARCH LABORATORY
AIR FORCE MATERIEL COMMAND
WRIGHT-PATTERSON AIR FORCE BASE, OH 45433-7750**

REPORT DOCUMENTATION PAGE

Form Approved
OMB No. 0704-0188

1. REPORT DATE *(DD-MM-YY)*	2. REPORT TYPE	3. DATES COVERED *(From - To)*
May 2006	Journal Article Preprint	

4. TITLE AND SUBTITLE

SILVER DIFFUSION AND HIGH-TEMPERATURE LUBRICATION MECHANISMS OF YSZ-Ag-Mo BASED NANOCOMPOSITE COATINGS (Preprint)

5a. CONTRACT NUMBER
F33615-01-D-5802

5b. GRANT NUMBER

5c. PROGRAM ELEMENT NUMBER
62102F

6. AUTHOR(S)

J.J. Hu (Nonstructural Materials Branch (AFRL/MLBT))
C. Muratore and A.A. Voevodin (UES, Inc.)

5d. PROJECT NUMBER
4349

5e. TASK NUMBER
LO

5f. WORK UNIT NUMBER
4349LOT3

7. PERFORMING ORGANIZATION NAME(S) AND ADDRESS(ES)

Nonstructural Materials Branch (AFRL/MLBT)
Metals, Ceramics and Nondestructive Evaluation Division
Materials and Manufacturing Directorate
Air Force Research Laboratory, Air Force Materiel Command
Wright-Patterson AFB, OH 45433-7750

UES, Inc.

8. PERFORMING ORGANIZATION REPORT NUMBER

9. SPONSORING/MONITORING AGENCY NAME(S) AND ADDRESS(ES)

Materials and Manufacturing Directorate
Air Force Research Laboratory
Air Force Materiel Command
Wright-Patterson AFB, OH 45433-7750

10. SPONSORING/MONITORING AGENCY ACRONYM(S)
AFRL-ML-WP

11. SPONSORING/MONITORING AGENCY REPORT NUMBER(S)
AFRL-ML-WP-TP-2006-454

12. DISTRIBUTION/AVAILABILITY STATEMENT
Approved for public release; distribution is unlimited.

13. SUPPLEMENTARY NOTES
Submitted for publication in *Composites Science and Technology*. PAO Case Number: AFRL/WS 06-1565, 20 June 2006. Paper contains color.

14. ABSTRACT
Yttria-stabilized zirconia (YSZ) nanocomposite coatings consisting of silver and molybdenum were produced by a hybrid process of filtered vacuum arc, magnetron sputtering and pulsed laser depositions for tribological investigations at different high temperatures. The microstructure of the coatings was determined by X-ray diffraction and transmission electron microscopy. The friction coefficients were measured using a high-temperature ball-on-disk tribometer at 25 to 700°C. The coatings with 24 at.% Ag and 10 at.% Mo contents showed a friction coefficient of 0.4 or less for all temperatures from 25 to 700°C. The wear scar surfaces and coating cross sections were studied using scanning electron, transmission electron, scanning transmission electron and focused ion beam microscopes, which provided the information on chemical composition distributions of silver and molybdenum along with microstructure features. The silver diffusion and coalescence on surfaces played an important part in the high-temperature lubrication mechanism of the YSZ-Ag-Mo coatings. Silver was found to be an effective lubricant at temperatures below 500°C and its coalescence on the surface isolated molybdenum inside coatings from ambient oxygen. Lubricious oxides of molybdenum were formed and lubricated at temperatures above 500°C when the silver was worn off the contact surface. For silver containment inside the coating at high temperatures, a multilayer architecture was build by inserting a TiN diffusion barrier layer in the composite coatings. Microscopic observations showed that this barrier layer prevented silver exit to the coating surface. At the same time, this enabled a subsequent lateral lubricant supply toward a wear scar location where the diffusion barrier layer was worn through and/or for a next thermal cycle. The multilayer coating maintained a friction coefficient of 0.4 or less for more than 25,000 cycles, while the monolithic coating lasted less than 5,000 cycles. In addition, a TiN surface barrier layer with pinholes was deposited on the YSZ-Ag-Mo composite surface to control vertical silver diffusion. With this coating design, the coating wear lifetime was significantly increased beyond 50,000 cycles. The heating-induced silver diffusion in lateral and vertical directions, silver coalescence on coating surfaces, molybdenum oxidation inside wear tracks, and diffusion-controlling TiN diffusion barrier layers are responsible for reduced friction and wear of these composite coatings at high temperatures.

15. SUBJECT TERMS
Yttria-stabilized zirconia, nanocomposite, multilayer, silver, molybdenum, high-temperature lubrication, focused ion beam

16. SECURITY CLASSIFICATION OF:			17. LIMITATION OF ABSTRACT:	18. NUMBER OF PAGES	19a. NAME OF RESPONSIBLE PERSON (Monitor)
a. REPORT Unclassified	**b. ABSTRACT** Unclassified	**c. THIS PAGE** Unclassified	SAR	48	Andrey A. Voevodin **19b. TELEPHONE NUMBER** *(Include Area Code)* (937) 255-5731

Standard Form 298 (Rev. 8-98)
Prescribed by ANSI Std. Z39-18

i

Silver diffusion and high-temperature lubrication mechanisms of YSZ-Ag-Mo based nanocomposite coatings

J.J. Hu[*], C. Muratore, A.A. Voevodin

Materials and Manufacturing Directorate, Air Force Research Laboratory (AFRL / MLBT), Wright-Patterson Air Force Base, Dayton, Ohio 45433-7750

* Author to whom all correspondence should be addressed (JJH) 937-255-3312 phone, 937-255-2176 fax; Email: Jianjun.Hu@WPAFB.AF.MIL

Jianjun Hu
AFRL / MLBT, Bldg. 654
2941 Hobson Way, Room 08
WPAFB, OH 45433-7750

Abstract

Yttria-stabilized zirconia (YSZ) nanocomposite coatings consisting of silver and molybdenum were produced by a hybrid process of filtered vacuum arc, magnetron sputtering and pulsed laser depositions for tribological investigations at different temperatures. The microstructure of the coatings was determined by X-ray diffraction and transmission electron microscopy. The friction coefficients were measured using a high-temperature ball-on-disk tribometer from 25 to 700 $^{\circ}$C. The coatings with 24 at.% Ag and 10 at.% Mo contents showed a friction coefficient of 0.4 or less for all temperatures from 25 to 700 °C. The wear scar surfaces and coating cross sections were studied using scanning electron, transmission electron, scanning transmission electron and focused ion beam microscopes, which also provided the information on chemical composition distributions of silver and molybdenum along with microstructure features. It was demonstrated that silver diffusion and coalescence on surfaces played an important part in the high-temperature lubrication mechanism of the YSZ-Ag-Mo coatings. Silver was found to be an effective lubricant at temperatures below 500 $^{\circ}$C and its coalescence on the surface isolated molybdenum inside coatings from ambient oxygen. Lubricious oxides of molybdenum were formed and lubricated at temperatures above 500 $^{\circ}$C when the silver was worn off the contact surface. For silver containment inside the coating at high temperatures, a multilayer architecture was built by inserting a TiN diffusion barrier layer in the composite coatings. Microscopic observations showed that this barrier layer prevented silver exit to the coating surface. At the same time, this enabled a subsequent lateral lubricant supply toward a wear scar location where the diffusion barrier layer was worn through and/or for a next thermal cycle. The multilayer coating maintained a

friction coefficient of 0.4 or less for more than 25,000 cycles, while the monolithic coating lasted less than 5,000 cycles. In addition, a TiN surface barrier layer with pinholes was deposited on the YSZ-Ag-Mo composite surface to control vertical silver diffusion. With this coating design, the coating wear lifetime was significantly increased beyond 50,000 cycles. The heating-induced silver diffusion in lateral and vertical directions, silver coalescence on coating surfaces, molybdenum oxidization inside wear tracks, and diffusion-controlling TiN diffusion barrier layers are responsible for reduced friction and wear of these composite coatings at high temperatures.

1. Introduction

Yttria-stabilized zirconia (YSZ) based nanocomposite coatings have received growing attention for their remarkable properties such as high hardness, toughness, wear resistance and low friction [1-13]. These properties are highly desirable for aerospace applications in order to increase the lifetime and performance of mechanical systems. The nanocomposite structure of the coatings provided a "chameleon" surface adaptation in addition to excellent mechanical and thermal stability of YSZ ceramic itself, which was previously studied for surface wear protection at different test environments, contact loads, sliding speeds, and temperatures [14-20]. The aerospace materials require a very demanding self-adapting performance to a wide range of environments and temperatures. The "chameleon" coating concept was developed with a series of tribological adaptive nanocomposite coatings consisting of amorphous and nanocrystalline phases, which can transform into lubricants when exposed to changes in environments and temperatures [8, 21-23]. Proper sized nanocrystalline grains can restrict crack size, create a large volume of grain boundaries, and hence improve the coating toughness and contact load support [24, 25]. The nanocomposite coatings consisting of YSZ ceramics and noble metals were initially studied for tribological uses at high temperatures [6-9].

The early investigations of YSZ-Au nanocomposite coatings showed that soft ductile gold was able to provide a low friction for up to 500 ^{o}C [6]. The weak bonding between ceramic and metallic components can facilitate the grain boundary sliding and improve the composite toughness. The in-situ transmission electron microscopy studies of YSZ-Au nanocomposites during heating showed that the diffusion process was

accompanied by the coating microstructural and chemical changes [9]. Increased temperatures initiated the crystallization and growth of zirconia and gold nanograins inside the coatings and formation of 100-500 nm gold islands on the coating surfaces. A primary mechanism for the friction reduction of YSZ-Au coatings was based on the low shear deformation of the surface gold islands under friction-induced stress. Recently, YSZ-Ag-Mo nanocomposite coatings were produced by a hybrid process of magnetron sputtering and pulsed laser depositions [10, 11]. Silver is an effective lubricant at moderately high temperatures [26-31], and molybdenum-based compounds are lubricious at higher temperatures in air, as shown by other researchers [32-36]. The YSZ-Ag-Mo coatings provided lubrication by forming a silver rich surface at 300-500 $^{\circ}$C and by oxide formation in friction contact at above 500 $^{\circ}$C. Studies on the YSZ-Ag-Mo coatings have been conducted on growth, characterization, mechanical and tribological properties.

The noble metals such as gold and silver have a large diffusion coefficient and high mobility at elevated temperatures. Heating activates diffusion out of highly strained sites in the YSZ matrix to open surfaces, where the reduction of system potential and surface energies thermodynamically drives metal grain nucleation and growth. After the noble metal transport to the surface, the coating becomes depleted in the lubricious metal and can not act as a self-lubricated composite for long. Control of such diffusion processes is, hence, needed for an extended lubrication. Transition metal nitrides were reported as effective diffusion barrier materials for noble metals [37]. The wear lifetime of YSZ-Ag-Mo nanocomposite coatings was shown to be significantly increased when using a TiN diffusion barrier to restrict the silver diffusion [12, 13]. For such composite coatings, the high temperature tribological performance strongly depends on the

thermodynamic activation of silver diffusion in the coating matrix, diffusion process control with barrier layers, tribochemical reactions in the contact surface, and structural stability of the ceramic matrix.

In this paper, we focused on the microstructure evolution, silver diffusion development, and contact surface oxidation processes for a series of YSZ-Ag-Mo based nanocomposite coatings in sliding contacts at high temperatures in air. The silver diffusion behavior in the coatings after heating was directly observed by using electron microscopes. Focused ion beam (FIB) microscope was used to set-up observations of microstructural and chemical studies in coating cross sections. Such experiments have not been reported in detail or used in tribological investigations before. The friction coefficients were measured at different high temperatures, and were examined in a close relationship with the coating surface changes in microstructure and chemistry. The results of our investigations reveal different high-temperature-adaptive lubrication mechanisms in the nanocomposite "chameleon" coatings.

2. Experimental

The YSZ-Ag-Mo nanocomposite coatings were produced with a hybrid process of filtered vacuum arc, magnetron sputtering and pulsed laser deposition in a stainless steel chamber, as shown in Figure 1. The chamber was evacuated using a 520 ls^{-1} turbo pump to a base pressure of 7 x 10^{-6} Pa or less. Mirror polished M50 steel and Inconel 718 super-alloy substrates of 25 mm diameter were ultrasonically degreased and loaded into the chamber. The substrates were heated to 150 ^{o}C, and then bombarded with energetic

argon ions (800 eV) and metal ions (650 eV) to clean the surface before deposition. A thin titanium adhesion layer (< 100 nm) was deposited on substrates by using the filtered titanium vacuum arc plasma. Pulsed laser deposition of YSZ was then initiated with a laser pulse repetition rate gradually ramped from 1 to 30 Hz to produce a graded Ti/YSZ transition layer and further promote the coating adhesion to the substrates. A KrF excimer laser (LPX300 Lambda Physik) produced 800 mJ, 25 ns width UV pulses (248 nm). The laser beam was directed by a set of programmable mirrors to random positions on a rotating YSZ target. The chamber was then filled with 1.6 Pa Ar (99.99% pure) at a flow rate of 100 sccm to facilitate sputtering. Silver and molybdenum were added to the coatings by magnetron sputtering from metal targets made of pure silver and pure molybdenum. The dc power density on the both magnetron targets was adjusted from 1 to 5 W cm^{-2} in order to control metal contents in the produced composite YSZ-Ag-Mo coatings. During deposition, the substrates were biased to -150 V dc, and maintained at 150 $^{\circ}$C. For multilayer architectures, a 100 nm thick TiN diffusion barrier layer was reactively deposited between two 1 μm thick YSZ-Ag-Mo layers by flowing 30 sccm nitrogen into the chamber while operating the filtered titanium arc plasma source. All coatings were grown to a thickness of approximate 2 μm in one to two hours depending on the magnetron power density. X-ray photoelectron spectroscopy (XPS) was used to determine that the YSZ-Ag-Mo coatings contained 5 to 24 atomic percent of Ag and 9 to 24 atomic percent of Mo. The TiN coatings were determined to be stoichiometric.

X-ray diffraction (XRD) data of the coatings were collected using a Rigaku diffractometer equipped with a monochromator in front of the Cu $K\alpha$ X-ray source.

Glancing incidence XRD was done with θ fixed at 8° for all scans in order to reduce the signal from substrates. Standard powder XRD patterns of tetragonal (*t*) ZrO2 and face-centered cubic (*fcc*) Ag were used for data interpretation [38, 39]. Transmission electron microscope (TEM) observations were performed using a Philips CM200 FEG (Field Emission Gun) microscope operated at 200 kV accelerating voltage. The FEG provided a complete coherent electron source and nm-sized probe, which were especially important for the high-spatial-resolution microstructure characterization. A NORAN x-ray energy dispersive spectrometer (EDS) was installed on the TEM and was used for chemical microanalyses of the coatings.

Friction coefficients in air with 40% (±1%) relative humidity (RH) were measured with a high-temperature (HT) ball-on-disk tribometer at 25, 300, 500 and 700 ^{o}C. Silicon nitride balls of 6.35-mm-diameter and 1 N normal load were used for all tests (approximate 0.7 GPa initial Hertzian contact stress). The tribotests were started after the coating samples were heated to the desired temperatures in about 20-35 minutes, and allowed to equilibrate for 5-10 minutes. Upon completion of the ball-on-disk measurements, samples were immediately removed from the furnace and allowed to cool in air. A series of annealing experiments were also performed using the same HT tribometer oven.

After tribotests, wear scars and sample surfaces were examined using a Leica 360 FEG scanning electron microscope (SEM) operating at 25 kV, which was equipped with a Link ISIS system of EDS for chemical analyses. A focused ion beam (FIB) microscope, FEI-DB235, was used to prepare lift-out specimens for showing the cross-sectional microstructure of the coatings. It was operated using 5 keV electron beams and

30 keV Ga$^+$ ion beams. To protect the coating surface, an approximately 2 μm thick Pt cap was deposited on the top of the samples using a gas injection system at a moderate ion beam current. Scanning transmission electron microscopy (STEM) and TEM/EDS were employed to study the cross-sectional microstructure and chemistry of the coatings after annealing. All these measurements were performed in order to understand the lubrication mechanism of YSZ-Ag-Mo nanocomposite coatings at high temperatures.

3. Results and discussion

3.1. Studies of structure evolution and lubrication mechanisms in YSZ-Ag-Mo composite coatings

Pure metallic Ag and Mo were added into the YSZ coatings at a different atomic percentage to reach desirable mechanical and tribological properties of the coatings [10, 11]. Figure 2 shows the XRD spectra of the YSZ-Ag-10 at.% Mo composite coatings containing 5, 16 and 24 at.% Ag, which exhibit weak tetragonal zirconia peaks and stronger cubic silver peaks. The intensity of t-ZrO$_2$ (111) peaks decreased with increasing silver contents, while the molybdenum diffraction was not detected. The strong silver peaks dominated the XRD spectra from the coatings with higher silver contents, and the Fe (110) peaks from M50 steel substrates were obscured by the Ag (200) peaks. Silver nanograins are visible in the high-resolution TEM image, as shown in Figure 3. The corresponding selected-area electron diffraction (SAED) pattern exhibits

diffraction rings indexing randomly oriented t-ZrO_2 and fcc-Ag phases, as shown in Figure 3 – insert.

Figure 4 shows the friction coefficients of the YSZ-Ag-Mo composite coatings grown with 5 to 24 at.% silver contents and 10 at.% molybdenum content at room to high temperatures. The 5 at.% Ag coating exhibited high friction at all temperatures, and the 17 at.% Ag coating exhibited a high friction at 500 °C and over. The 24 at.% Ag coating had a friction coefficient of 0.4 or less for all temperatures from 25 to 700 °C. Therefore, a sufficient amount of silver in the coating is required to facilitate lubrication at high temperatures. Unless otherwise noted, the YSZ-Ag-Mo composites in the following analyses and discussions contained 24 at.% Ag and 10 at.% Mo.

Coating wear tracks after sliding tests at 500 °C and prior to coating failure were analyzed using SEM/EDS (Figure 5). Smeared regions were found inside wear tracks, which were predominantly composed of silver, as shown in Figure 5(a). A high magnification image of the smeared silver film is shown in Figure 5(b). EDS elemental mappings of Ag, Zr, Mo and Fe (Figure 5(c)) reveal the silver-covered regions on the surface as Ag is in bright contrast, while Zr and Mo are visible on the silver-worn-off surfaces as Zr and Mo are in bright contrast. The weak Fe signal contrast resulted from steel substrates being under a less thick YSZ-Ag-Mo layer in worn wear track areas.

After 1000 cycles of sliding tests at 700 °C, some oxidization products like MoO_3 were found inside the wear track between smeared silver regions, as shown in Figure 6. MoO_3 demonstrates a low shear stress at 700 °C and has been recommended to use as a lubricant at high temperatures. Figure 6 also shows the coverage of the coating surface outside wear track with heating-induced silver surface layer, which was disrupted inside

wear tracks since silver, as a lubricant, does not work well above 500 $^{\circ}$C. The thermodynamic activation of silver diffusion is inevitable during HT sliding. Results of the silver diffusion studies in the YSZ-Mo-Ag composite coatings after heating are discussed next.

Figures 7(a) and (b) show the SEM images taken from (a) the cross-sectional specimen of the coating as cut in a FIB microscope, and (b) the coating surface outside the wear track after heating to 500 $^{\circ}$C during tribometer tests. The initial monolithic YSZ-Ag-Mo composite coating developed into two distinct layers after heating, as shown in Figure 7(a), where a platinum cap was deposited on the coating surface for protection during FIB sample preparation. EDS measurements determined that the chemical composition of the bright top layer was silver. The lower layer was a sliver-depleted coating, which mainly consisted of YSZ and molybdenum. Dense silver grains of 1-2 microns in size grew, coalesced, and completely covered the coating surface after heating, as shown in Figure 7(b). The grains are significantly larger than the initial silver nanograins in the as-deposited coatings (compare to figure 3).

XRD patterns were measured from the annealed coatings in order to further investigate the coating microstructure evolution during heating. Narrower *fcc*-Ag (111) and (200) peaks developed after annealing in comparison to the as-deposited coating, as shown in Figure 8, which indicated a largely increased grain size of silver. In addition, a well-defined *t*-ZrO_2 (111) peak was found for the annealed coating pattern, which was nearly invisible in the as-deposited coating. Low temperature growth of YSZ-Ag-Mo composites in this study possibly resulted in a formation of solid solutions of silver and molybdenum in highly defective and distorted zirconia nanocrystalline grains in addition

to silver grains. At equilibrium conditions, silver is immiscible with zirconia and, hence, it would diffuse out of zirconia lattice defects under temperature activation. This process was accompanied by zirconia lattice relaxation, ordering and crystallization, and was evidenced by the XRD pattern in Figure 8.

Figure 9 provides a schematic diagram of silver diffusion stages in heating sequences to facilitate a discussion on the thermodynamic behavior of silver inside the nanocomposite matrix. As produced, silver exists as nanocrystalline grains inside YSZ-Ag-Mo nanocomposites and as metastable solid solution inside defected zirconia lattice (first stage – right in Figure 9). This is a distinct difference in comparison to the distribution of large silver grains (first stage – left in Figure 9) in macrocomposites, for example, produced by plasma spay techniques, such as the NASA PS200 and PS300 series high temperature lubricating coatings [28, 29]. At the same volume of silver contents, there are two major factors that thermodynamically accelerate silver diffusion in nanocomposites as compared to macrocomposites: (1) a much larger surface area of the embedded silver nanograins provides a significantly larger decrease in grain boundary surface energy by the grain coalescence; and (2) a much shorter distance between the embedded silver nanograins makes the grain growth kinetic much faster.

From the above considerations, YSZ-Ag-Mo nanocomposite coatings require less heating energy for the silver atoms to overcome the potential barrier and cover the distance between neighboring silver grains for their growth. In addition to the silver diffusion, the heating activates zirconia structure ordering and crystallization (Figure 8). This ordering process pushes inserted silver atoms out of the defects inside zirconia grains. However, the YSZ-Ag-Mo coatings produced in this study are dense and free of

voids to accommodate space requirements for the silver grain growth, in contrast to typical porosity and voids in plasma sprayed macrocomposite coatings. This creates a space restriction for the silver grain growth inside the nanocomposite coating matrix. Such space for the silver grain growth is available at the coating surface and vertical silver diffusion transports the silver from the coating bulk to the surface for the silver grain formation and growth (Fig. 7b). This heating-induced silver diffusion and coalescence in YZS-Ag-Mo nanocomposite coatings provide a thermodynamically driven mechanism for the formation of a dense silver layer on the coating surface, which seals a silver-depleted YSZ-Mo composite layer inside the coating (final stage in Figure 9).

3.2. Silver diffusion control and lubrication mechanisms in multilayered YSZ-Ag-Mo/TiN coatings

In an effort to increase the coating endurance and move toward thermal cycling capability, a multilayer architecture was produced by interleaving a 100 nm thick TiN diffusion barrier in YSZ-Ag-Mo composites, as schematically shown in Figure 10(a) [12]. A thin (<50 nm) titanium adhesion layer with Ti-YSZ graded compositions was deposited between the TiN barrier layer and top YSZ-Ag-Mo composite layer. Also, a thin (<50 nm) Ag-Mo layer was deposited under the TiN layer to direct the silver composition gradient downward. This Ag-Mo underlayer also provided lubrication upon initial contact of the ball with the coating under the TiN layer at the moment when it was breached in the wear process. This multilayer architecture provided a fresh layer of composite lubricants after the TiN barrier layer was worn through, as shown in Figure

10(b). The lateral diffusion of silver from within the lower composite layer toward the relatively small wear scar provides a continuous supply of the lubricant (compare 10-100 μm typical wear track width with 10-100 mm typical substrate surface dimensions). This can considerably increase the coating wear lifetime [12]. Figure 11 shows the friction traces of both monolithic and multilayer YSZ-Ag-Mo coatings in sliding tests at 500 $^{\circ}$C in air. The YSZ-Ag-Mo/TiN multilayer coating maintained a friction coefficient of approximately less than 0.4 for over 25,000 cycles, while the YSZ-Ag-Mo monolithic coating could only provide lubrication for about 4,500 cycles. The present results demonstrate the benefit of the multilayer composite design to increase the coating endurance for HT lubrications.

The multilayer coating microstructure after heating to 500 $^{\circ}$C was further studied using a TEM. Figure 12(a) shows a TEM image of the coating cross section as prepared by lift-out in a FIB microscope. The top silver layer was formed by the heating-induced silver diffusion and coalescence on surfaces from the upper YSZ-Ag-Mo layer of the multilayer composite coating – similar as discussed in the Section 3.1. Micron-sized columnar silver crystals grew on the surface, as indicated in Figure 12(a). Figure 12(b) shows a SAED pattern taken from one of the silver grains. The pattern consists of individual diffraction spots of a single crystal indexing *fcc*-Ag (111) and (200) planes.

A silver-depleted YSZ-Mo composite layer remained beneath the silver surface after the silver diffusion to the coating surface. A SAED pattern from this silver-depleted YSZ-Mo layer is shown in figure 12(c). The diffraction rings were indexed to t-ZrO$_2$ (111), (220), and (113) planes with random orientations in the layer. The heating effects caused the crystallization of zirconia, which was more like an amorphous phase in the as-

deposited composite coatings. These TEM results of the top YSZ-Ag-Mo composite layer are in a good agreement with the above SEM and XRD studies as discussed in the Section 3.1 and shown in Figures 7 and 8.

In contrast to the changes of the upper YSZ-Ag-Mo layer, there was no detectable chemical composition change in the YSZ-Ag-Mo layer under the TiN barrier layer. The chemical compositions of the different layers were measured by the EDS elemental mappings of Ag, Zr, Ti, Mo, O and Fe, as shown in Figure 12(d). From these analyses, it was confirmed that the chemical compositions were well maintained in the lower YSZ-Ag-Mo layer deposited under the TiN barrier layer. Cross-sectional TEM of the annealed multilayer coating did not show visible morphology and structural changes inside this lower composite layer in comparison to the as-deposited coating.

Therefore, YSZ-Ag-Mo/TiN multilayer design helped to increase wear life by the restriction of silver diffusions in a vertical direction and created conditions for guiding subsurface silver diffusion laterally toward the wear scar area. This novel lateral diffusion mechanism is very beneficial for HT lubrication and extends lubricant supply to the wear track over longer time periods. It can be easily controlled through an optimization of the individual composite layer thickness (defines diffusion cross section area) and the number of layers in the coating stack (defines total availability of the preserved lubricant reservoirs). Also, the insertion of dense and thin TiN barrier layers is an efficient way to prevent undesirable permanent changes in microstructures and chemistries in the depth of underlying YSZ-Ag-Mo composite layers. This enhances the overall coating stability and endurance in HT applications.

3.3. Retardation of silver surface release via a porous TiN barrier "mask"

Instead of a dense TiN barrier interlayer for completely sealing the underneath YSZ-Ag-Mo composite, a TiN barrier surface layer with a random array of pinholes – a porous TiN (p-TiN) "mask" – was produced to prolong the wear lifetime of the YSZ-Ag-Mo composite coatings [13]. This approach restricted the lubricant transport to the coating surface through those holes and reduced the silver depletion rate at high temperatures. Figure 13(a) shows a schematic structural design of the coating with a p-TiN diffusion barrier mask, and (b) shows a SEM image taken from the TiN/YSZ-Ag-Mo coating with pinholes on the p-TiN surface. The silver diffusion paths by heating are schematically shown in Figure 13(c). Dome-like silver islands formed on the surface (Figure 13(d)), after the coating was heated to 500 $^{\circ}$C in the tribometer furnace and maintained at that temperature for 45 minutes. The size of the islands was varied within approximate 10-50 μm. The SEM results demonstrated that the p-TiN barrier mask restricted the silver transport to the surface, as compared to the unrestricted silver diffusion out of YSZ-Ag-Mo coatings discussed in Section 3.1 and shown in Figure 7.

Figure 14 shows the friction trace of the above TiN/YSZ-Ag-Mo coating in the ball-on-disk tests at 500 $^{\circ}$C. For comparison purposes, monolithic YSZ-Ag-Mo and dense monolithic TiN coatings of the same total thickness as the TiN/YSZ-Ag-Mo coating were also measured under the same tribotest conditions. The monolithic YSZ-Ag-Mo coating showed a steady-state friction coefficient of 0.4 before failure at 4,500 cycles, as indicated by a sudden increase in friction coefficients. The friction coefficient of the TiN coating was maintained at 0.5 for 12000 cycles before increasing to 0.65,

which was consistent with the friction coefficient of uncoated M50 steel substrates at 500 $^{\circ}$C. The TiN/YSZ-Ag-Mo coating did not fail in our tests over 50,000 cycles, and it maintained a friction coefficient of approximate 0.4. Therefore, a significant extension of the wear lifetime was demonstrated for the coating covered with a p-TiN barrier mask, which helped to restrict the silver diffusion to the surface and to reduce the depletion rate of silver in under-surface coating volumes.

For further studying the silver diffusion mechanisms in YSZ-Ag-Mo composites under a p-TiN barrier mask, cross-sectional specimens were prepared using a FIB to cut sections in the middle of dome-like silver islands, as shown in Figure 15 (a). In-situ lift-out of the thin foils of coating cross sections was performed by using an Omniprobe manipulator attached to FIB, as shown in Figure 15(b). Electron transparent specimens were finally produced by ion beam polishing the section foils welded on Omniprobe grids. Figure 15(c) shows a SEM image of the above FIB-cut coating cross section, and Figure 15(d) shows the corresponding dark field (DF) STEM image, which was taken by using an annular STEM detector installed under the specimen. EDS analyses determined that the dome-like islands formed on the surface consisted of pure silver while zirconia and molybdenum were maintained inside the coating body. Figures 15(e) and (f) show the EDS elemental mapping results for Ag and Ti, respectively. Diffusion affected regions inside YSZ-Ag-Mo composite layer, which were sandwiched between adhesive Ti and barrier p-TiN layers, are clearly visible in those images.

The SEM image shows the silver regions in bright contrast and some columnar silver crystals are indicated by arrows in Figure 15(c). The columnar crystal growth of silver can also be visible in the insert SEM image taken from the top of the sample. The

DF-STEM image showed the silver regions in dark contrast and was more sensitive to the variation of silver contents. From these analyses, the silver-depleted region in the coating was reasonably defined, as indicated in Figures 15(d) and (e). The region width was measured as approximate 12 μm. Beyond this region, the silver composition was maintained unchanged and could act as a subsequent lubricant reservoir. These silver atoms will take longer time (more than 45 minutes of this annealing experiment) to diffuse out of the coating to the surface.

These microstructure characterizations provided the evidence of the lateral silver diffusion mechanism from inside the coating toward the holes of the p-TiN barrier mask and then vertically to the surface with a grain growth on the exit of the p-TiN layer holes. The silver surface release was restricted by the size and surface area density of holes in the p-TiN layer. This mechanism explains why the thin p-TiN barrier mask can provide a multifold increase of the YSZ-Ag-Mo coating endurance during HT sliding in air.

4. Conclusions

YSZ-Ag-Mo nanocomposite coatings were produced by combining filtered vacuum arc, magnetron sputtering and pulsed laser depositions. They maintained a friction coefficient of approximate 0.4 or less for all the temperatures from 25 to 700 °C during HT ball-on-disk tribometer tests. The XRD and TEM analyses of as-deposited coatings determined their nanocomposite structure consisted of silver nanograins embedded in an amorphous/nanocrystalline YSZ-Mo matrix. At high temperatures, the heating-induced silver diffusion and coalescence resulted in coating microstructure and

chemistry changes with a granular silver film formed on the coating surface and a silver-depleted YSZ-Mo layer left underneath. Zirconia matrix crystallization occurred in parallel with silver surface diffusion when the coating was heated. It was confirmed that the silver diffusion and coalescence on the surface played an important part for HT lubrication mechanisms of YSZ-Ag-Mo nanocomposite coatings. Silver was an effective lubricant at temperatures below 500 $^\circ$C, and the silver coalescence on surfaces isolated molybdenum inside the composites from ambient oxygen. At temperatures above 500 $^\circ$C, the silver cap layer was rapidly removed from wear tracks and hence the reactive molybdenum inside the silver-depleted YSZ-Mo layer was exposed to ambient air. Contact tribochemistry resulted in the formation of molybdenum oxides in wear tracks, which provided lubrication at 700 $^\circ$C.

For controlling silver diffusion, multilayer-structured coatings were prepared by inserting a dense TiN diffusion barrier layer between two YSZ-Ag-Mo nanocomposite layers. This TiN barrier preserved lubricants underneath for a continuous lubricant replenishment and forced a subsurface silver to diffuse laterally toward the wear scars, once the TiN layer was breached by wear. Such a mechanism provided an adaptive system response with "on demand" lubricant supply from storage volumes inside YSZ-Ag-Mo composites to the surface contact areas. These multilayer YSZ-Ag-Mo/TiN coatings maintained a friction coefficient of approximately 0.4 for more than 25,000 cycles, while the monolithic YSZ-Ag-Mo coatings lasted less than 5,000 cycles. Finally, a p-TiN barrier mask was coated on the YSZ-Ag-Mo composite surface to reduce the silver diffusion rate to the surface as demonstrated by FIB microscopic studies. The wear lifetime of p-TiN barrier masked coatings was increased beyond 50,000 cycles, and was

significantly longer than that of monolithic YSZ-Ag-Mo or dense TiN coatings. The present studies establish basic mechanisms and concept foundation for developing YSZ-Ag-Mo nanocomposite coatings with dense TiN barrier interlayers and porous TiN surface masks for HT sliding in air with moderately low friction and long lifetime.

Acknowledgements

References

1. Voevodin AA, Jones JG, Zabinski JS. J Appl Phys 2000; 88: 1088.

2. Voevodin AA, Jones JG, Zabinski JS. Appl Phys Lett 2001; 78: 730.

3. Voevodin AA, Jones JG, Zabinski JS. J Vac Sci Technol A 2001; 19(4): 1320.

4. Jones JG, Voevodin AA, Zabinski JS. Surf Coat Technol 2001; 146: 258.

5. Voevodin AA, Jones JG, Zabinski JS. Laser Ablation, Low Temperature Fabricated Yttria-Stabilized Zirconia Oriented Films. US Patent # 6,509, 070; January 21, 2003.

6. Voevodin AA, Hu JJ, Fitz TA, Zabinski JS. Surf Coat Technol 2001; 146: 351.

7. Voevodin AA, Hu JJ, Jones JG, Fitz TA, Zabinski JS. Thin Solid Films 2001; 401: 187.

8. Voevodin AA, Fitz TA, Hu JJ, Zabinski JS. J Vac Sci Technol A 2002; 20(4): 1434.

9. Hu JJ, Voevodin AA, Zabinski JS. J Mater Res 2005; 20: 1860.

10. Muratore C, Voevodin AA, Hu JJ, Jones JG, Zabinski JS. Surf Coat Technol 2005; 200: 1549.

11. Muratore C, Voevodin AA, Hu JJ, Zabinski JS. Wear 2006; in press.

12. Muratore C, Voevodin AA, Hu JJ, Zabinski JS. Tribology Letters 2006; in press.

13. Muratore C, Hu JJ, Voevodin AA. Thin Solid Films 2006; in press.

14. Fischer TE, Anderson MP, Jahanmir S, Salher R. Wear 1988; 124: 133.

15. Fischer TE, Anderson MP, Jahanmir S. J Am Ceram Soc 1989; 72: 252.

16. Stachowiak GW, Stachowiak GB. Wear 1989; 132: 151.

17. Stachowiak GW, Stachowiak GB. Wear 1991; 143: 277.

18. Carter GM, Hooper RM, Henshall JL, Guillou MO. Wear 1991; 148: 147.

19. Lee SW, Hsu SM, Shen MC. J Am Ceram Soc 1993; 76: 1937.

20. Tucci A, Esposito L. Wear 1994; 172: 111.

21. Voevodin AA, O'Neill JP, Zabinski JS. Surf Coat Technol 1999; 119: 36.

22. Voevodin AA, Zabinski JS. Thin Solid Films 2000; 370: 223.

23. Voevodin AA, Zabinski JS. Composite Science and Technology 2005; 65: 741.

24. Veprek S, Reiprich S, Li SZ. Appl Phys Lett 1995; 66: 2640.

25. Musil J, Zeman P, Hruby H, Mayrhofer PH. Surf Coat Technol 1999; 120/121: 179.

26. Sliney HE. Tribol Int 1982; 15: 303.

27. Sliney HE. ASLE Trans 1985; 29: 370.

28. DellaCorte C, Sliney HE. Lubrication Engineering 1991; 47: 298.

29. DellaCorte C. Surf Coat Technol 1996; 86/87: 486.

30. Erdemir A, Erck RA, Fenske GR, Hong H. Wear 1997; 203/204: 588.

31. Endrino JL, Nainaparampil JJ, Krzanowski JE. Surf Coat Technol 2002; 157: 95.

32. Peterson MB, Murray SF, Florek JJ. ASLE Trans 1959; 2: 225.

33. Murray SF, Calabrese SJ. Lubrication Engineering 1992; 49: 955.

34. Wahl KJ, Seitzman LE, Bolster RN, Singer IL. Surf Coat Technol 1997; 89: 245.

35. Woydt M, Skopp A, Dorfel I, Witke K. Wear 1998; 218: 84.

36. Strong KL, Zabinski JS. Thin Solid Films 2002; 406: 174.

37. Nicolet MA. Thin Solid Films 1978; 52: 415.

38. PDF Card#27-0997. JCPDS Powder Diffraction File (International Center for Powder Diffraction Data, Swarthmore, PA, 1998).

39. PDF Card#04-0783. JCPDS Powder Diffraction File (International Center for

   Powder Diffraction Data, Swarthmore, PA, 1998).

Figure captions

Fig. 1.   Schematic diagram of the deposition chamber, combining filtered vacuum arc, magnetron sputtering, and pulsed laser deposition.

Fig. 2.   XRD spectra of YSZ-Ag-Mo composite coatings with different Ag contents and 10 at.% Mo. Spectra are shifted on the vertical scale for clarity.

Fig. 3.   High-resolution TEM image and the corresponding SAED pattern taken from the YSZ-24 at.% Ag-10 at.% Mo composite coating.

Fig. 4.   Friction coefficients of YSZ-Ag-Mo composite coatings with different Ag contents and 10 at.% Mo from room to high temperatures.

Fig. 5.   (a) SEM image taken from the wear scar surface after friction coefficient measurements at 500 °C prior to coating failure. (b) High magnification image of a smeared Ag film inside the wear track. (c) EDS elemental mappings of Ag, Zr, Mo and Fe. The silver-covered regions on the wear scar surface show bright contrast in the Ag mapping.

Fig. 6.   SEM image taken from the wear scar surface after 1000 cycles of tribometer tests at 700 °C. MoO_3 grains exist inside the wear track along with smeared silver films.

Fig. 7.   (a) Cross-sectional micrograph and (b) surface micrograph of the YSZ-24 at.% Ag-10 at.% Mo composite coating after heating to 500 °C as observed using a FIB microscope.

Fig. 8.   XRD spectra of the YSZ-24 at.% Ag-10 at.% Mo composite coating before (dotted line) and after (solid line) heating. The inset is a zoom-in pattern of the (111) Zr_2O diffraction region.

Fig. 9.   Schematic diagram of the thermodynamic migration of silver inside the YSZ-Ag-Mo nanocomposite coating after heating.

Fig. 10. (a) Schematic of the multilayer structure divided by a TiN diffusion barrier layer. (b) Schematic of the expected response of the multilayer coating during high-temperature tribotests.

Fig. 11. Friction trace of the multilayer YSZ-Ag-Mo/TiN coating in the ball-on-disk test at 500 ^{o}C. The friction trace of monolithic YSZ-Ag-Mo coating measured under the same conditions is shown for comparison.

Fig. 12. (a) TEM image of the multilayer YSZ-Ag-Mo/TiN coating cross section after heating to 500 ^{o}C. (b) SAED pattern taken from the top silver layer. (c) SAED pattern taken from the silver-depleted YSZ-Mo composite layer.   (d) EDS elemental mappings of Ag, Zr, Ti, Mo, O, and Fe recorded for the same coating cross section as shown in (a).

Fig. 13. (a) Schematic of the coating structure design with a TiN diffusion barrier mask on the surface. (b) SEM image showing the TiN/YSZ-Ag-Mo coating prepared with micron pinholes on the surface. (c) Schematic illustration of the heating-induced silver diffusion path in the coating. (d) SEM image showing dome-like silver islands formed on the surface after heating at 500 ^{o}C for 45 minutes.

Fig. 14. Friction trace of the TiN-barrier-masked TiN/YSZ-Ag-Mo coating in the ball-on-disk test at 500 $^{\circ}$C. The friction traces of monolithic YSZ-Ag-Mo and TiN coatings measured under the same conditions are shown for comparisons.

Fig. 15. (a) SEM image of a dome-like silver island on the TiN-barrier-masked TiN/YSZ-Ag-Mo coating surface after heating to 500 $^{\circ}$C, in which a white box indicates the cross section position for FIB cutting. (b) In-situ lift-out of the thin foil of the coating cross section. (c) SEM image taken from the coating cross section showing silver regions in bright contrast. Inset is a SEM image taken from the top of the sample. (d) DF-STEM image of the coating cross section showing silver regions in dark contrast with a high sensitivity to silver concentrations. (e) and (f) EDS elemental mappings of Ag and Ti recorded for the same coating cross section as shown in (c).
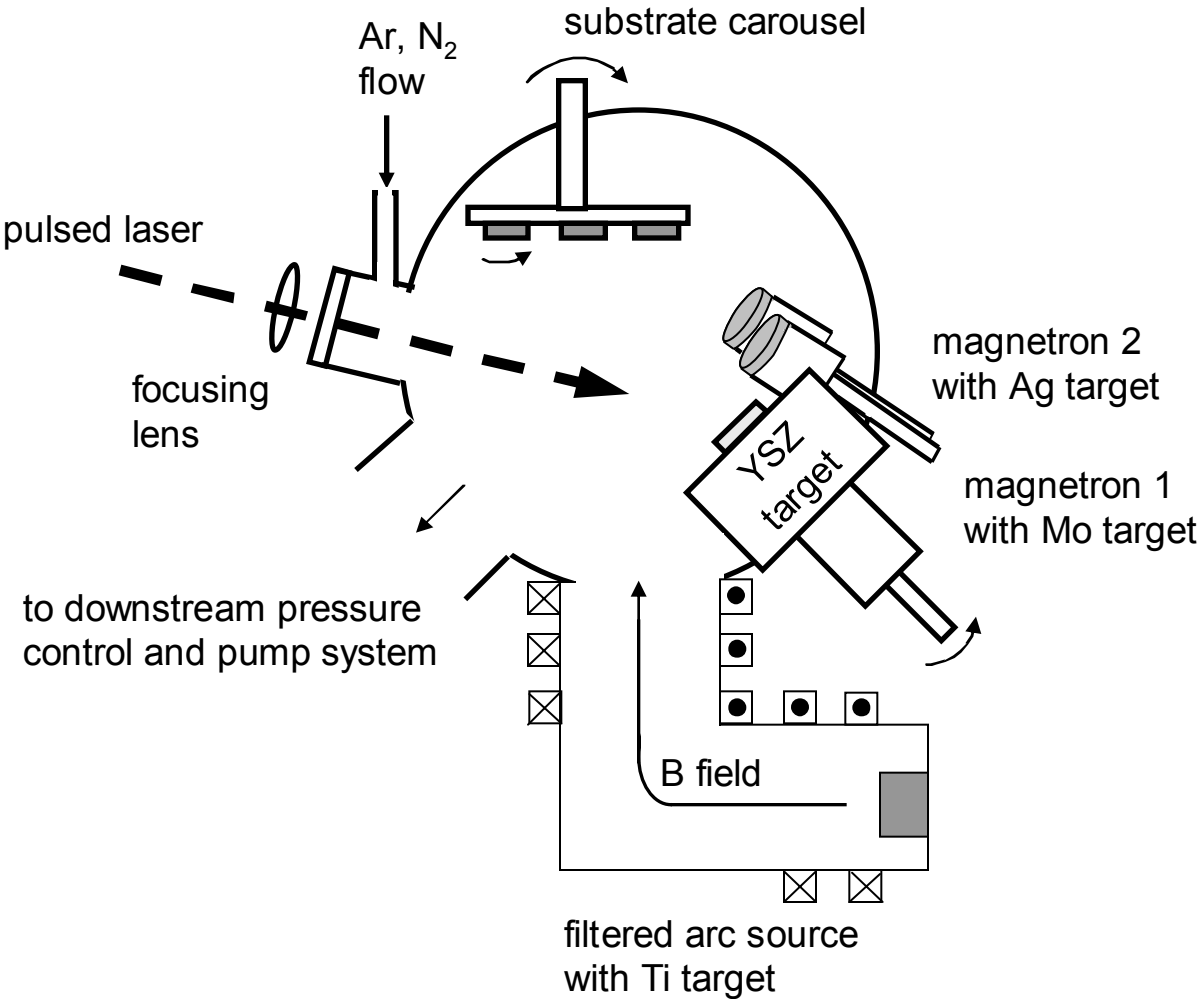
Figure 1
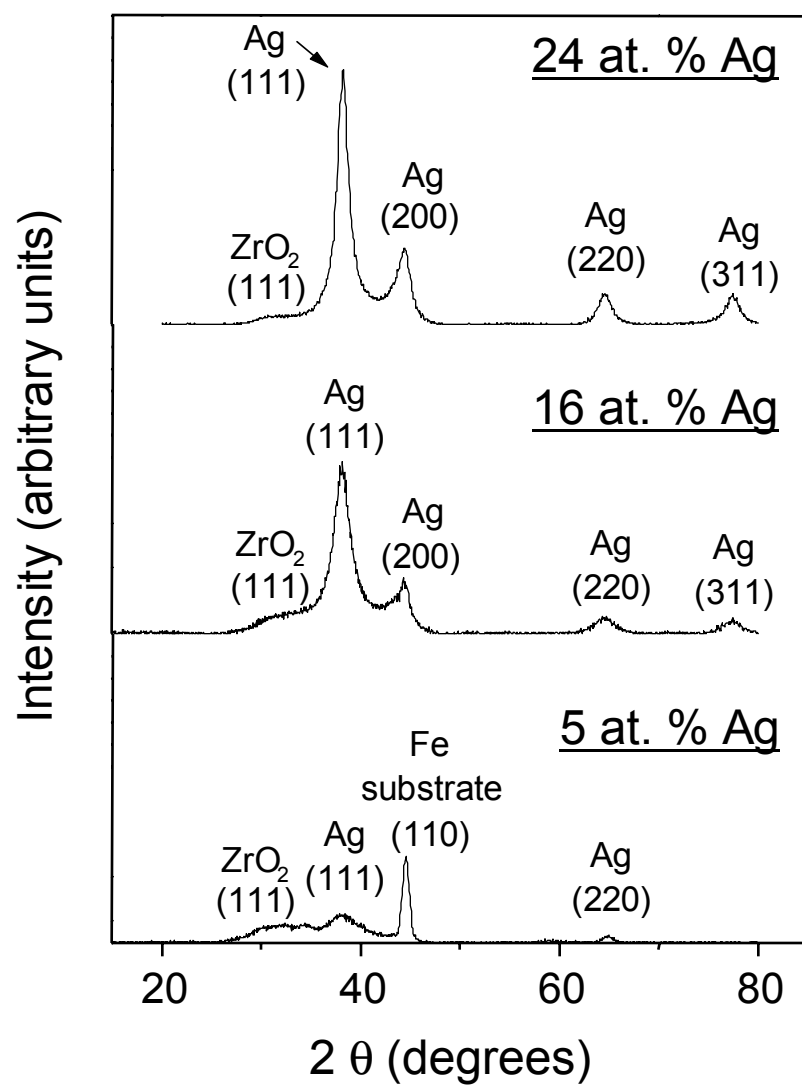
Figure 2

Figure 3

Figure 4

(a)

100μm

Sliding direction

Ag film

Wear scar

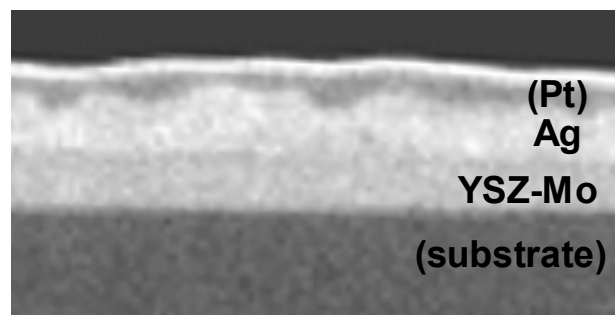(b)
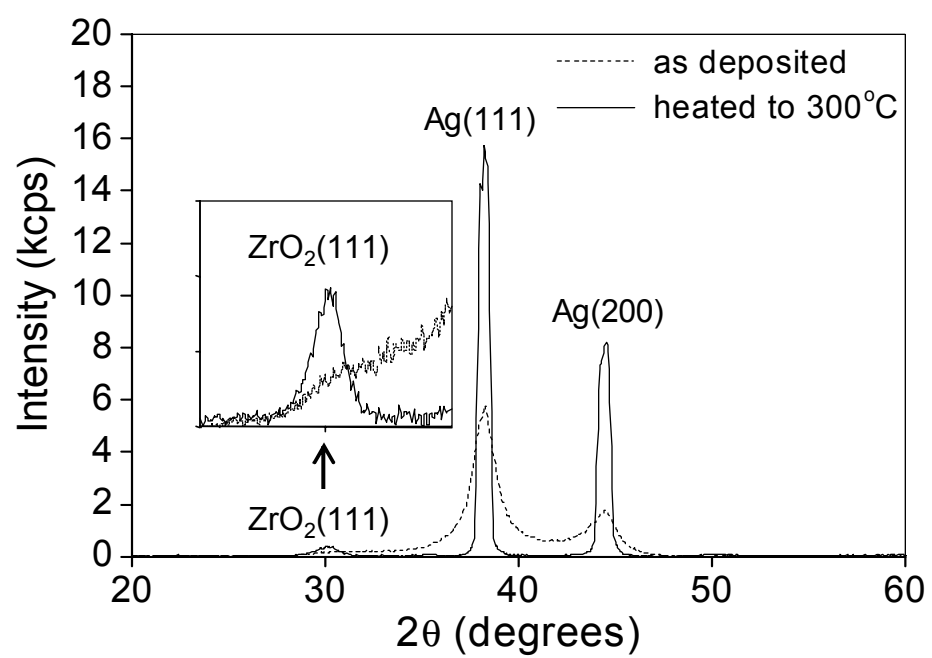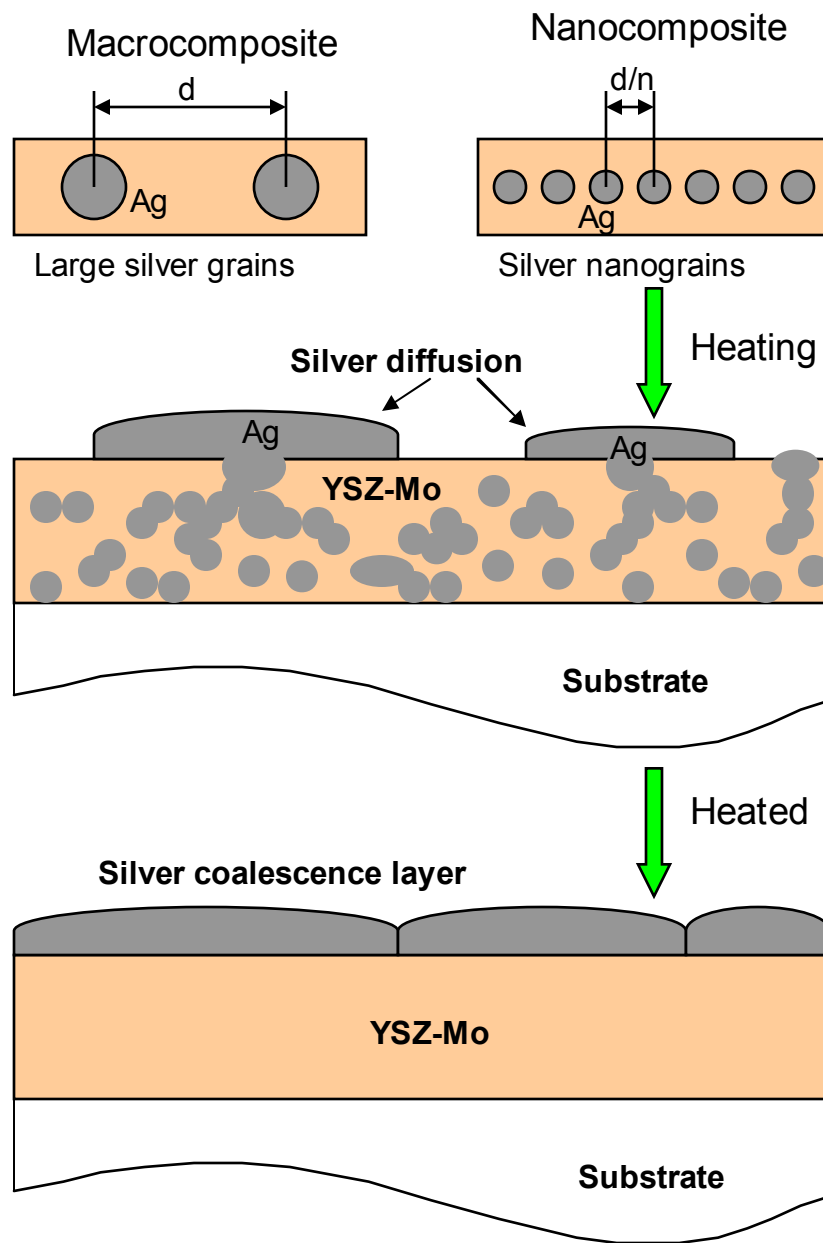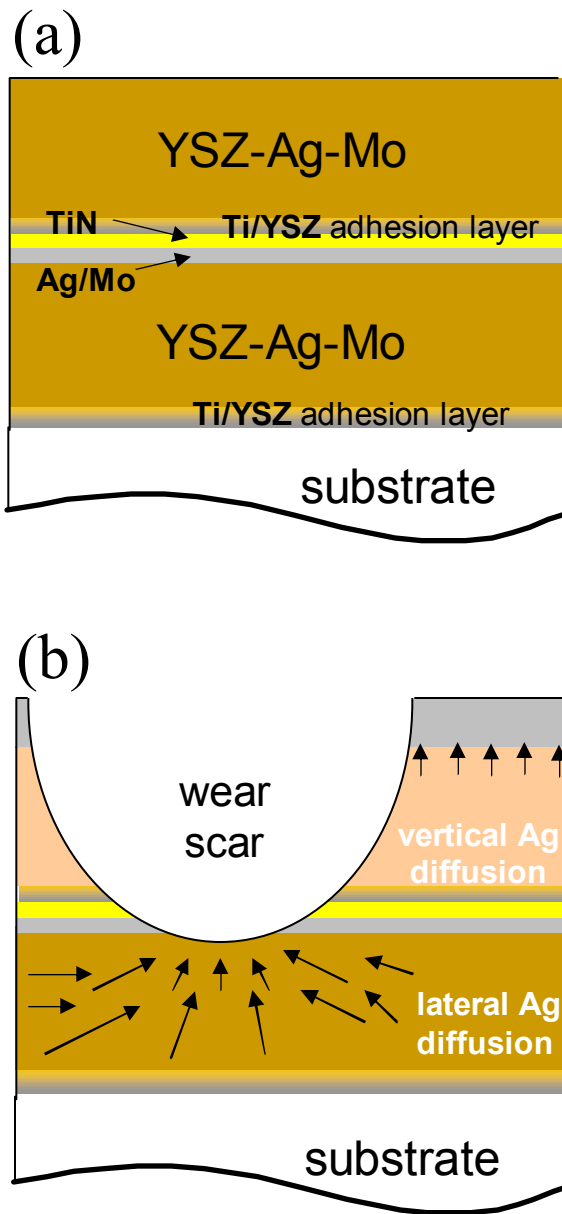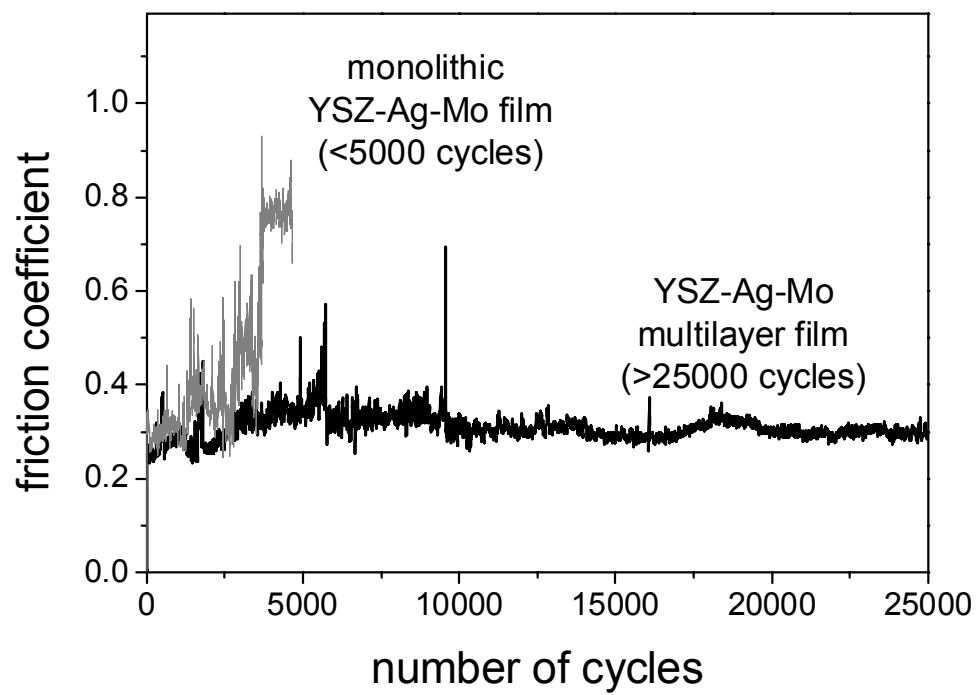
Ag film

20μm

(c)

Ag

Zr

Mo

Fe

Figure 5

Figure 6

(Pt)
Ag
YSZ-Mo
(substrate)

2µm

(a)

2µm
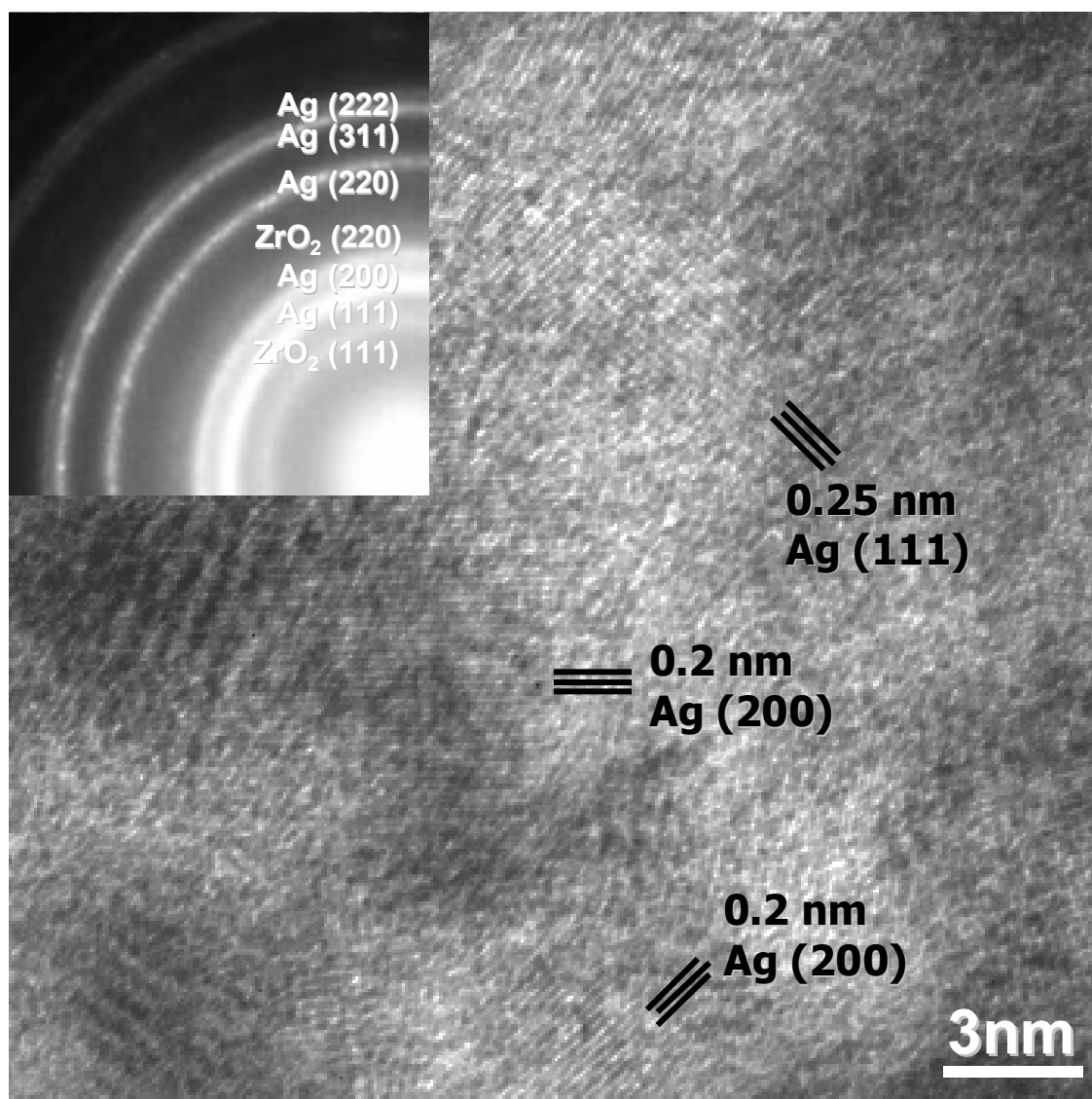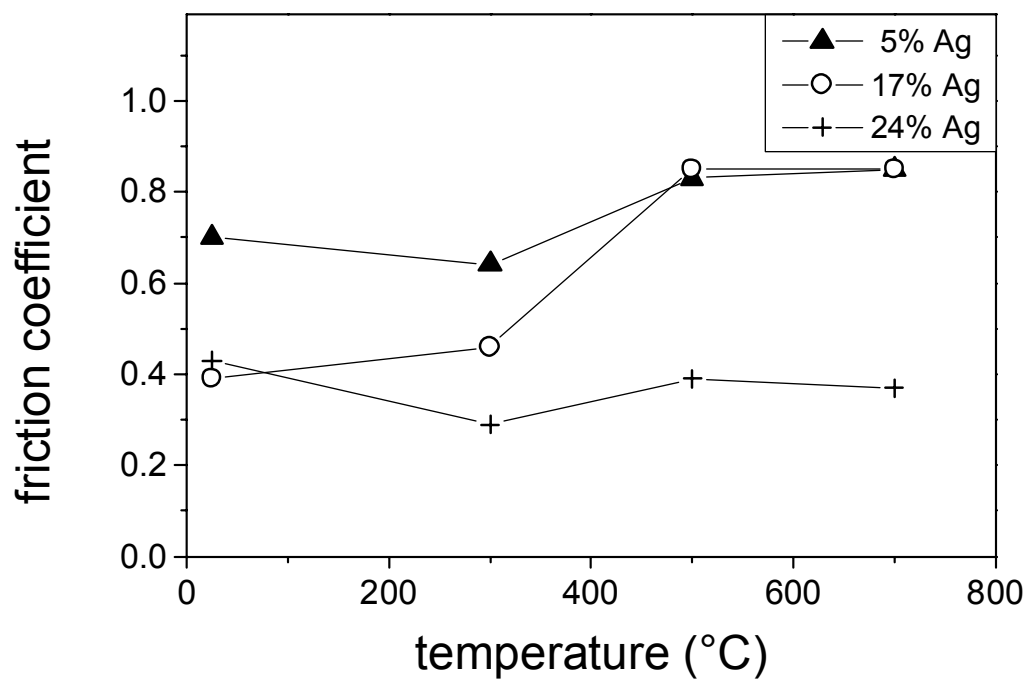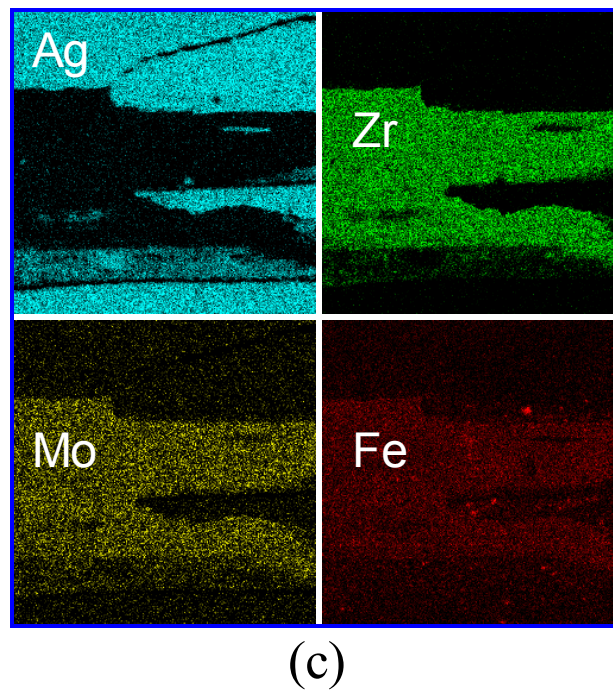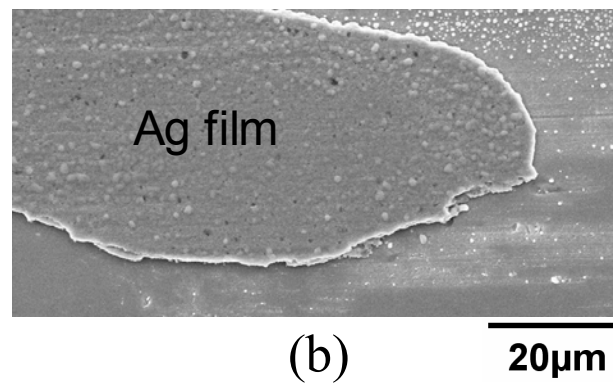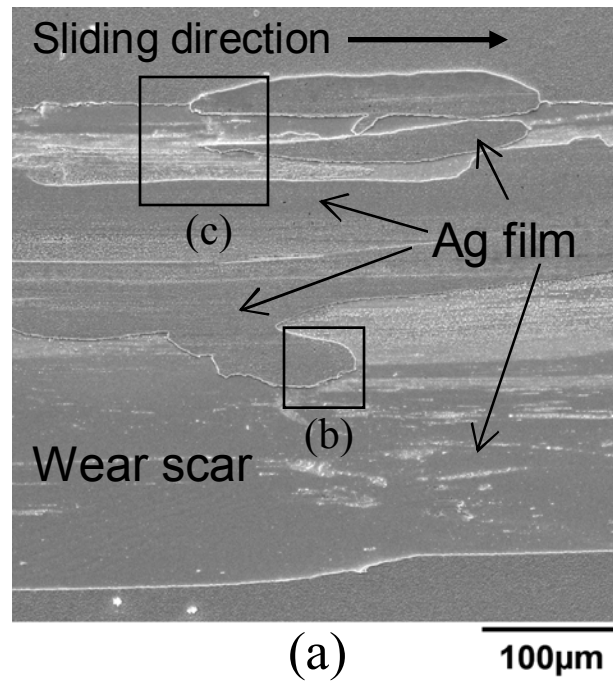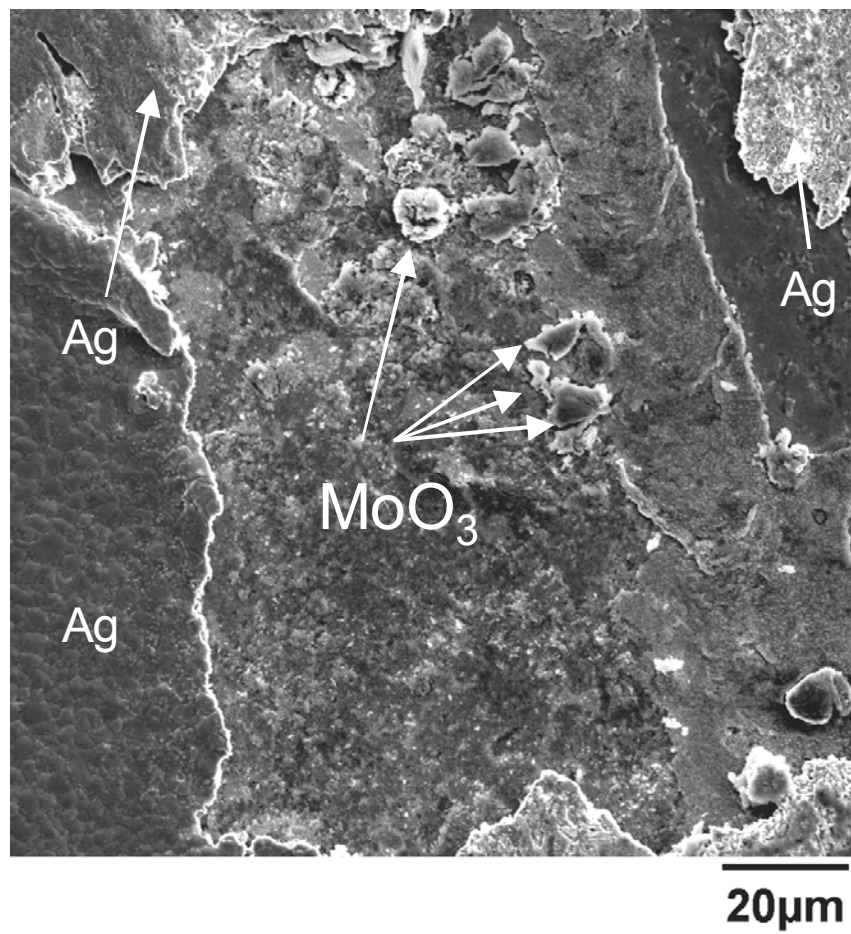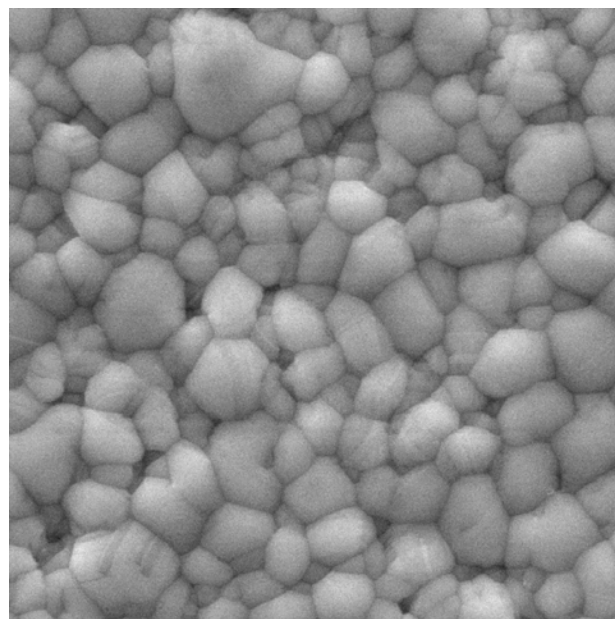
(b)

Figure 7

Figure 8

Figure 9

(a)

YSZ-Ag-Mo

TiN → Ti/YSZ adhesion layer

Ag/Mo

YSZ-Ag-Mo

Ti/YSZ adhesion layer

substrate

(b)

wear scar

vertical Ag diffusion

lateral Ag diffusion

substrate
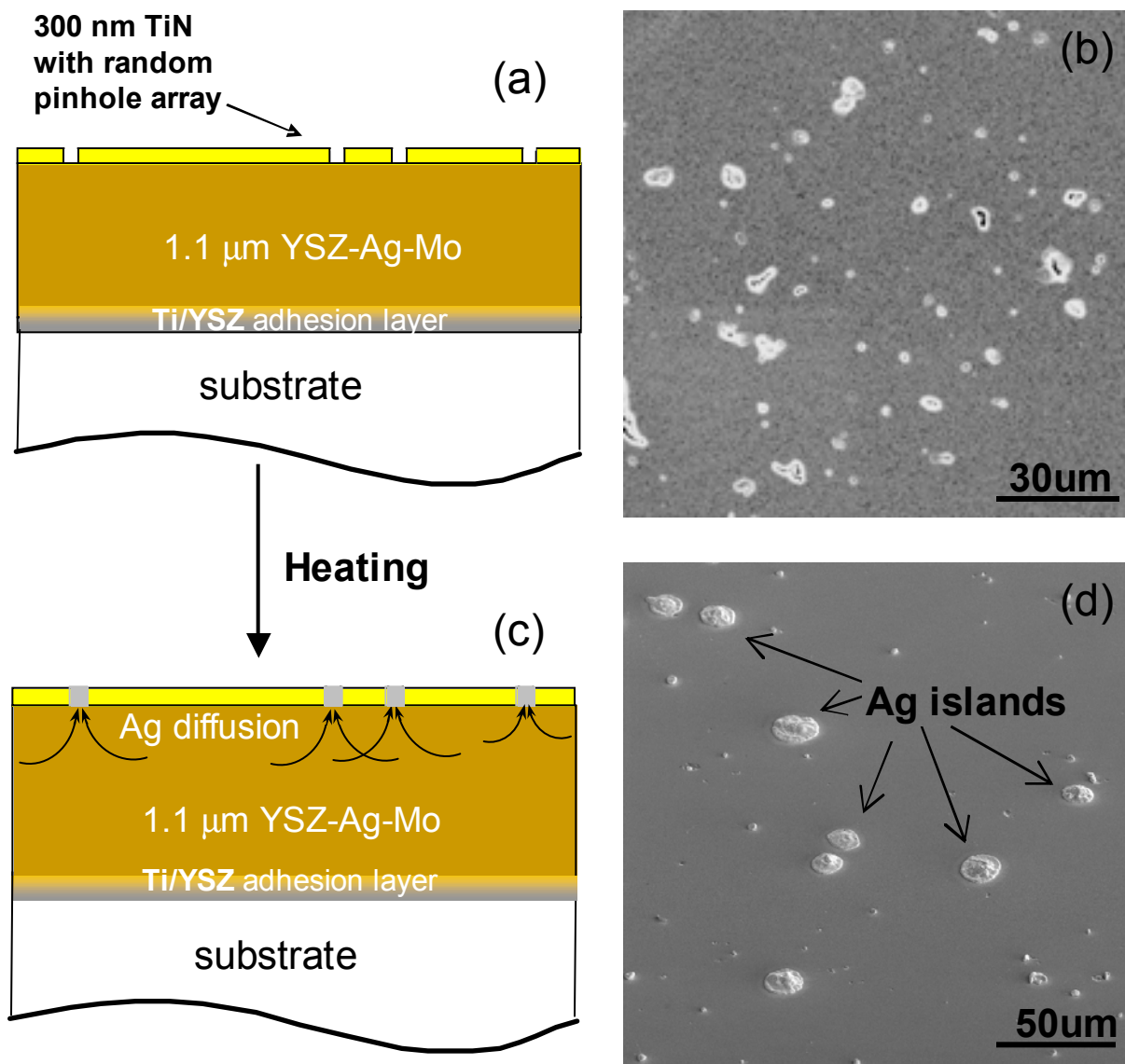
Figure 10

Figure 11

Figure 12

300 nm TiN
with random
pinhole array

(a)

1.1 μm YSZ-Ag-Mo

Ti/YSZ adhesion layer

substrate

Heating

(c)

Ag diffusion

1.1 μm YSZ-Ag-Mo

Ti/YSZ adhesion layer

substrate

(b)

30um

(d)

Ag islands

50um

Figure 13

Figure 14

(a)

5 um

(b)

1um

E-Beam
5.00 kV

Scan
6.34 s

20 μm

Ag crystals

(c)

(Pt)

Ag
TiN

YSZ-Mo

YSZ-Ag-Mo

(substrate)

2 um

(d)

(Pt)

Ag
TiN

YSZ-Mo

YSZ-Ag-Mo

Ag depleted region

(substrate)

2 um

(e)

Ag

Ag depleted region

(f)

Ti

Figure 15

41